Phase Diagram of Mg Insertion into Chevrel Phases, $Mg_xMo_6T_8$ (T = S, Se). 1. Crystal Structure of the Sulfides

E. Levi,[†] E. Lancry,[†] A. Mitelman,[†] D. Aurbach,[†] G. Ceder,[‡] D. Morgan,[§] and O. Isnard[||,⊥]

Department of Chemistry, Bar-Ilan University, Ramat-Gan, Israel 52900, Department of Materials Science and Engineering, Massachusetts Institute of Technology, Cambridge, Massachusetts 02139, Department of Materials Science and Engineering, University of Wisconsin−Madison, Madison, Wisconsin 53706, Laboratoire de Cristallographie, Université J. Fourier CNRS, BP166X, 38042 Grenoble Cedex 9, France, and Institut Laue Langevin, BP 156 X, 38042 Grenoble Cedex 9, France

Received July 17, 2006. Revised Manuscript Received September 12, 2006

A combination of ab initio calculations and experimental methods (high-resolution neutron and powder X-ray diffractions) was used to solve the crystal structure of $Mg_xMo_6S_8$ ($x = 1$ and 2). It was shown that at room temperature, the latter are similar to the crystal structure of classic Chevrel phases (CPs) such as $Cu_xMo_6S_8$: space group $R\bar{3}$, $a_r = 6.494$ Å, $\alpha = 93.43°$ for $MgMo_6S_8$ and $a_r = 6.615$ Å, $\alpha = 95.16°$ for $Mg_2Mo_6S_8$. For $x = 1$, one Mg^{2+} cation per formula unit is distributed statistically between inner sites. For $x = 2$, the second Mg^{2+} cation per formula unit is located in the outer sites. Peculiarities of the electrochemical behavior of the CPs as electrode materials for Mg batteries were understood on the basis of the analysis of the interatomic distances. It was shown that the circular motion of the Mg^{2+} ions between the inner sites in $MgMo_6S_8$ is more favorable than their progressive diffusion in the bulk of the material, resulting in relatively slow diffusion and Mg trapping in this phase. In contrast, in $Mg_2Mo_6S_8$, the repulsion between the Mg^{2+} ions located in the inner and outer sites facilitates their transport through the material bulk.

Introduction

Chevrel phases (CPs) have been intensively studied in the last three decades as superconductors, catalysts, thermoelectric materials, and cathodes in Li batteries.[1−6] In addition to their ability for monovalent insertion (Li^+, Na^+, Cu^+), these unusual compounds allow for a fast transport of divalent cations, such as Zn^{2+}, Cd^{2+}, Ni^{2+}, Mn^{2+}, Co^{2+}, and Fe^{2+}.[7−10] Recently, it was found that this impressive list could be extended to a strongly polarizing Mg^{2+} ion.[11−13] As was shown, the Mg transport in the CPs is so fast that, in contrast to other hosts, these materials do not need special preparation in the form of nanomaterials to be used as practical cathodes in rechargeable Mg batteries. However, the kinetics of the Mg diffusion in the CPs is strongly affected by their composition and temperature. At ambient temperature, the selenide shows excellent Mg mobility in the full intercalation range from zero to two Mg^{2+} ions per formula unit,[14] whereas Mg trapping happens in the sulfide, i.e., the essential part of the Mg^{2+} ions (about 25%) can be removed from the crystal structure of Mo_6S_8 only at elevated temperatures.[15]

In general, in order to understand the kinetics problems of ion motion in the intercalation compounds, it is necessary to analyze the diffusion pathway of the ion's insertion into the host.[16−19] It is clear that such an analysis is impossible without knowledge of the crystal structure of the intercalation compounds, which includes not only the atomic arrangement in the host but also the occupation of the cation sites. In the case of the CPs, the atomic arrangement of the host is well-known. It is a stacking of Mo_6T_8 blocks composed of the octahedral cluster of molybdenum atoms inside the anion

* Corresponding author. E-mail: elena1@mail.biu.ac.il.
[†] Bar-Ilan University.
[‡] Massachusetts Institute of Technology.
[§] University of Wisconsin−Madison.
[||] Université J. Fourier CNRS.
[⊥] Institut Laue Langevin.

(1) Yvon, K. In *Current Topics in Material Science*; Kaldis, E., Ed.; Elsevier: North-Holland, Amsterdam, 1979; Vol. 3.
(2) *Topics in Current Physics: Superconductivity in Ternary Compounds I*; Fisher. Ø., Maple, M. B., Eds.; Springer-Verlag: Berlin, 1982.
(3) Brorson, M.; King, J. D.; Kiriakidou, K.; Prestopino, F.; Nordlander, E. *Met. Cluster Chem.* **1999**, *2*, 741.
(4) Caillat, T.; Fleurial, J. P., Snyder, G. *J. Solid State Sci.* **1999**, *1*, 535.
(5) Nunes, R. W.; Mazin, I. I.; Singh, D. *J. Phys. Rev. B* **1999**, *59*, 7969.
(6) Schollhorn, R. *Angew. Chem., Int. Ed.* **1980,** *19*, 983.
(7) Fischer, C.; Gocke, E.; Stege, U.; Schollhorn, R. *J. Solid State Chem.* **1993**, *102*, 54.
(8) Tarascon, J. M.; Hull, G. W.; Marsh, P.; Ter Haar *J. Solid State Chem.* **1987,** *66*, 204.
(9) Gocke, E.; Schramm, W.; Dolscheid, P.; Schollhorn, R. *J. Solid State Chem.* **1987**, *70*, 71.
(10) Schollhorn, R.; Kumpers, M.; Besenhard, J. O. *Mater. Res. Bull.* **1977**, *12*, 781.
(11) Aurbach, D.; Lu, Z.; Schechter, A.; Gofer, Y.; Gizbar, H.; Turgeman, R.; Cohen, Y.; Moskovich, M.; Levi, E. *Nature* **2000**, *407*, 724.
(12) Aurbach, D.; Gofer, Y.; Lu, Z.; Schechter, A.; Chusid, O.; Gizbar, H.; Cohen, Y.; Ashkenazi, V.; Moskovich, Turgeman, R.; Levi, E. *J. Power Sources* **2001**, *97*, 28.
(13) Aurbach, D.; Weissman, I.; Gofer, Y.; Levi, E. *Chem. Rec.* **2003**, *3*, 61.
(14) Levi, M. D.; Lancry, E.; Levi, E; Gizbar, H.; Gofer, Y.; Aurbach, D. *Solid State Ionics* **2005**, *176*, 1695.
(15) Lancry, E.; Levi, E.; Gofer, Y.; Levi, M.; Salitra, G.; Aurbach, D. *Chem. Mater.* **2004**, *16*, 2832.
(16) West, A. R. *Basic Solid State Chemistry*; John Wiley & Sons: New York, 1988.
(17) Van der Ven, A.; Ceder, G. *Electrochem. Solid-State Lett.* **2000**, *3*, 301.
(18) Van der Ven, A.; Ceder, G.: Asta, M.; Tepesh, P. D. *Phys. Rev. B* **2001**, *6418*, 4307.
(19) Morgan, D.; Van der Ven, A.; Ceder, G. *Electrochem. Solid-State Lett.* **2004**, *7*, A30.

10.1021/cm061656f CCC: $33.50
Published on Web 10/18/2006 PAGE EST: 11.4

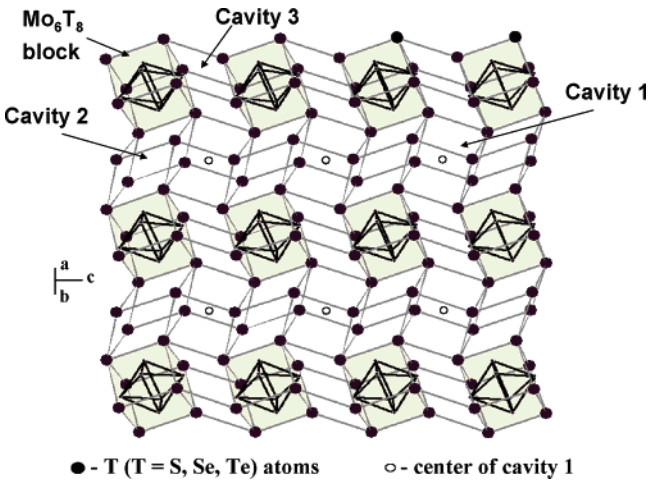

Figure 1. Three types of cavities in the CPs crystal structure. Dark cubes are Mo_6T_8 blocks.

cube. In contrast, a variety of different cation locations were discovered in the CPs.[1,2,20−26] From three types of cavities, formed between Mo_6T_8 blocks (Figure 1), only two of them (cavities 1 and 2) can be filled by cations of ternary metals, because a strong repulsion of the Mo atoms does not allow the occupation of cavity 3. In earlier works, devoted to the CPs, a simple scheme of the cation distribution was proposed.[1,2] According to this scheme, the cation position in the crystal structure depends mainly on its size. The big cations such as Pb^{2+} or Sn^{2+} (with a radius larger than 1 Å) occupy the center of the large cubic cavity 1, whereas the insertion of relatively small cations such as Cu^+ or Li^+ (with a radius smaller than 1 Å) leads to the deformation of the cubic anion environments around cations to the tetrahedral ones. These cavities form three-dimensional channels that are available for cation transport.

In classic CPs such as Cu- or Li-containing compounds, two types of the tetrahedral sites are used to describe the position of the small cations in the crystal structure: (1) so-called inner sites in cavity 1 that form a pleated ring and (2) outer sites in cavity 2 with a quasioctahedral arrangement.[1,2,20] In addition to the classic distribution, a new cation location in cavities 1 and 2 was recently found for selenides with small cations of transition metals.[21−24] Thus, the cation distribution in the crystal structure may be more complicated than the simple scheme proposed in earlier works. It depends on the specific interactions between the insertion cations and the Mo atoms of the cluster.

An important characteristic feature of the CPs in the case of small cations is the limit in the site occupancies. In fact, the cluster electronic structure allows for the maximal insertion of four monovalent cations (as in $Cu_4Mo_6T_8$), or two divalent cations (as in $Zn_2Mo_6T_8$) for each group of 12 sites (six inner and six outer sites) per cluster. In addition, the cation sites are located too close to each other and therefore cannot be occupied simultaneously because of the cation repulsion.

The specific occupation of the sites in $M_xMo_6T_8$ (M = metal) depends on the metal amount (x). In the case of low x, the inner sites are more favorable from a energetic point of view than the outer sites, because of the larger distances from the Mo atoms; therefore, they are usually occupied first. For instance, only the inner sites are occupied in $Cu_xMo_6T_8$ for $x < 2$ or in $Li_xMo_6S_8$ for $x = 1$. The occupation of the outer sites begins in $Cu_xMo_6T_8$ for $x > 2$ and in $Li_xMo_6S_8$ for $x > 1$, whereas the cation distribution in the inner sites remains unchanged.[20,25]

The site occupation also depends on the temperature.[1,2,26] At room temperature, small cations (<1 Å) in the classic CPs are distributed statistically between six available crystallographic positions, connected to each other by a -3-fold symmetric axis. As a result, the crystal symmetry is rhombohedral. At a low temperature, the transformation to triclinic symmetry may take place. In triclinic crystals, instead of six equivalent sites, there are only two, and they are connected to each other by the inversion center −1. In this case, dumbbells are used to describe the cation arrangement. The temperature of the phase transition depends on the CP composition, e.g., 270 K for $Cu_{1.8}Mo_6S_8$[26] and about 400 K for $Fe_2Mo_6S_8$.[1]

Thus, in spite of the fact that, in general, the basic crystal structure of the CPs is well-known, our crystallographic knowledge is not sufficient to predict the distribution of the Mg^{2+} ions in the cation sites or the stoichiometry and the symmetry of the Mg-containing CPs (MgCPs). In classic reviews,[1,2] it was mentioned that the exact crystal structure of $Mg_xMo_6S_8$ is not known. However, the MgCPs were cited as an example of nonstoichiometric compounds with rhombohedral symmetry for a low Mg concentration and triclinic symmetry for the Mg-rich phases.

An attempt at theoretically predicting the crystal structure of MgCPs was made using the density-functional technique.[27] According to this work, the sulfides, $Mg_xMo_6S_8$ ($x = 1$ and 2), should be triclinic, although this is really only a zero-temperature prediction. In contrast to the scheme of the cation arrangement presented in classic reviews,[1,2] the authors believe that the inner sites are occupied for $x = 2$, whereas for $x = 1$, the probabilities of the occupation for the inner and outer sites are equal.

In our previous experimental work,[15,28−31] we have studied MgCPs obtained by direct high-temperature synthesis and by electrochemical Mg insertion into a Mo_6S_8 host. It was shown[28] that the XRD patterns of the intercalation com-

(20) Ritter, C.; Gocke, E.; Fischer, C.; Schollhorn, R. *J. Mater. Res. Bull.* **1992**, *27*, 1217.
(21) Roche, C.; Chevrel, R.; Jenny, A.; Pecheur, P.; Scherrer, H.; Scherrer, S. *Phys. Rev. B* **1999**, *60*, 16442.
(22) Belin, S.; Chevrel, R.; Sergent, M. *J. Solid State Chem.* **2000**, *155*, 250.
(23) Mancour-Billah, A.; Chevrel, R. *J. Solid State Chem.* **2003**, *170*, 281.
(24) Mancour-Billah, A.; Chevrel, R. *J. Alloys Compd.* **2004,** *383*, 49.
(25) Yvon, K.; Paoli, A.; Flukiger, R.; Chevrel, R. *Acta Crystallogr., Sect. B* **1977**, *33*, 3066.
(26) Yvon, K.; Baillif, R.; Flukiger, R. *Acta Crystallogr., Sct. B* **1979**, *35*, 2859.
(27) Kganyago, K. R.; Ngoepe, P. E.; Catlow, C. R. A. *Phys. Rev. B* **2003**, *67*, 104103.
(28) Levi, E.; Lancry, E.; Gofer, Y.; Aurbach, D. *Solid-State Electrochem.* **2006**, *10*, 176.
(29) Levi, M. D.; Lancry, E.; Gizbar, H.; Gofer, Y.; Levi, E; Aurbach, D. *Electrochim. Acta* **2004**, *49*, 3201.
(30) Levi, M. D.; Gizbar, H.; Lancry, E.; Gofer, Y.; Levi, E.; Aurbach, D. *J. Electroanal. Chem.* **2004**, *569*, 211.
(31) Levi, M. D.; Lancry, E.; Gizbar, H.; Lu, Z.; Levi, E.; Gofer, Y.; Aurbach, D. *J. Electrochem. Soc.* **2004**, *151*, A1044.

pounds obtained by these different synthetic routes were identical, in spite of the presence of some minor additional diffraction peaks related to different impurities. According to this research,[15,29−31] the best way to determine the stoichiometry of the MgCPs is the electrochemical titration because of the atmospheric instability of the compounds.[28] However, such titration should be done at elevated temperature, because of the Mg trapping mentioned above. As was shown,[15,29−31] the electrochemical Mg insertion occurs in two stages

$$Mg^{2+} + 2e^- + Mo_6S_8 \rightarrow MgMo_6S_8 \quad (1)$$

$$Mg^{2+} + 2e^- + MgMo_6S_8 \rightarrow Mg_2Mo_6S_8 \quad (2)$$

Both of the phases were indexed as rhombohedral (space group $R\bar{3}$), with unit cell parameters $a = 9.445(6)$ Å, $c = 10.564(9)$ Å for $MgMo_6S_8$ and $a = 9.749(6)$ Å, $c = 10.374(9)$ Å for $Mg_2Mo_6S_8$.[15] Thus, there is no agreement among the researchers about the symmetry of the MgCPs and the location of the Mg^{2+} ions. Therefore, the question of the exact crystal structure of the MgCPs needs careful study.

The best method for determining the crystal structure is the XRD analysis of single crystals. However, the problem is that the Mg-containing CPs are stable only under special conditions, like a vacuum or parent solution (see the Experimental Section). Under air, and even in a special cell with Mylor film as an X-ray window, a self-Mg extraction from the crystal structure takes place. The material is stabilized only after formation of the compact passivating MgO films on its surface.[28] As a result, the XRD determinations based on the single crystals become problematic. Moreover, it is well-known that neutron diffraction is more convenient than X-ray diffraction when the positions of the light atoms should be determined.

Thus, the aim of this work was to refine the crystal structure of the MgCPs, i.e., determine the exact positions of the Mg^{2+} ions by a combination of experimental (Rietveld analysis based on neutron and X-ray diffractions) and theoretical (calculation of the energy of states) methods. On the basis of the crystal structure solutions, we analyzed the possible routes of the Mg^{2+} ions' transport in the MgCPs, in order to clarify the problems of ionic mobility in CPs, such as the relatively slow kinetics of the Mg insertion and Mg trapping in $Mg_xMo_6S_8$ for $0 < x < 1$. In addition, such a study completes our knowledge about structural diversity for this important class of materials.

Experimental Section

The preparation of the host, Mo_6S_8, as well as the electrochemical process for Mg insertion were described earlier.[15,29−31] $MgMo_6S_8$ for the Rietveld analysis was synthesized by reaction of the powder element mixture in an evacuated sealed quartz ampule. As was mentioned above, the exposure of MgCPs to air results in Mg extraction, which stops only after formation of the compact MgO surface films on the CP particles. Thus, in order to ensure the desirable stoichiometry after Mg extraction, the Mg concentration in the initial mixture was 1.5 times higher than the stoichiometric one. The ampule was heated up to 1100 °C for 72 h with additional steps at 450 and 700 °C, each for 24 h.

The material with the $Mg_2Mo_6S_8$ composition for the Rietveld analysis was synthesized via the topotactic reaction of the binary Mo_6S_8 in contact with a Ph_2Mg/THF solution as the source of Mg ions and as the reducing agent. Ph_2Mg was synthesized from PhMgCl (Aldrich) according to the Schlenk equilibrium

$$2RMgX \rightarrow R_2Mg + MgX_2$$

1,4-dioxane was used to shift the equilibrium to the right.

XRD studies were performed with a Bruker AXS (Germany) D8 ADVANCE diffractometer (reflection $\theta-\theta$ geometry, Cu K_α radiation, receiving slit 0.2 mm, scintillation counter), equipped with a Gobel mirror (parallel beam). Diffraction data were collected in the angular range of $10° < 2\theta < 110-140°$, step size 0.02°, step time 10 s/step.

The neutron diffraction experiments were performed at the Institut Laue Langevin (I.L.L.) at Grenoble, France, on the D1A instrument. A detailed description of this instrument is available via the Internet at http://www.ill.fr. D1A is a very high-resolution powder diffractometer operating with a take off angle of the monochromator of 122°. In the configuration used, the resolution of D1A is about 0.3° (FWHM) at 90°. The measurements were carried out at a wavelength of $\lambda = 1.911$ Å, selected by the (115) reflection of a germanium monochromator. During the neutron diffraction measurements, a cylindrical vanadium sample holder with an inner diameter of 7 mm was used. The neutron detection was performed with a set of 6° spaced 3He counting tubes. The complete diffraction pattern was obtained by scanning over the whole 2θ range.

The data were analyzed with the Rietveld structure refinement program, FULLPROF.[32] Agreement factors used in this article are defined according to the guidelines of the Rietveld refinement that can be found elsewhere.[33] The neutron scattering lengths used were $b_S = 0.2847 \times 10^{-14}$ m, $b_{Mg} = 0.5375 \times 10^{-14}$ m, and $b_{Mo} = 0.6715 \times 10^{-14}$ m; values were taken from the literature.[34]

Results and Discussion

Mg Insertion into Mo_6S_8 as a Two-Stage Process. The process of electrochemical Mg insertion into Mo_6S_8 was studied in detail in our previous works.[15,29−31] This paper is devoted to the crystal structure of the intercalation compounds. However, in order to illustrate the conclusions reached in the previous works and concerning the phase diagram of the $Mg-Mo_6S_8$ system, panels a and b of Figure 2 present the results of the electrochemical experiment and XRD phase analysis for the electrodes at different stages of Mg insertion.

In general, phase transitions in the insertion electrodes are associated with a constant potential on their chronopotential curves, whereas the stoichiometry of the intercalation compounds can be determined by the charge expended on their formation or by the lengths of the potential plateaus.[35] For insertion electrodes, the potential of the electrochemical reaction depends on the potential energy of the site occupancies in the crystal structure of the active material. Thus, a clear correlation exists between the electrochemical curve

(32) Rodriguez Carjaval, J. *Physica B* **1993**, *192*, 55.
(33) McCusker, L. B.; Von Dreele, R. B.; Cox, D. E.; Louer, D.; Scardi, P. *J. Appl. Crystallogr.* **1999**, *32*, 36.
(34) Sears, V. F. *Neutron News* **1992**, *3*, 26.
(35) *Lithium Batteries: Science and Technology*; Nazri, G. A.; Pistoia, G., Eds.; Kluwer Academic Publishers: Boston, 2004.

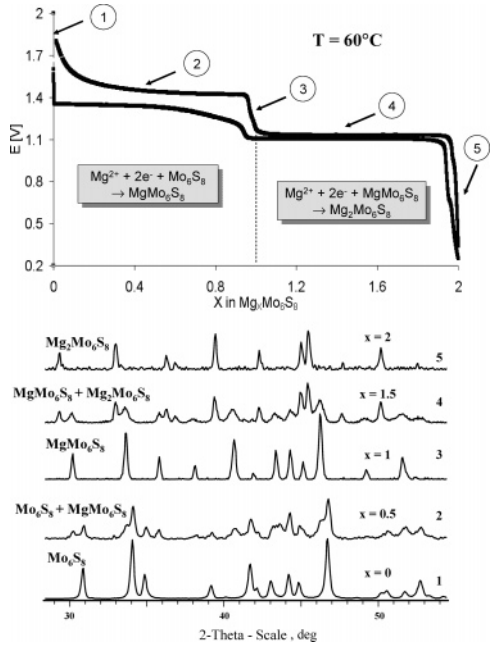

Figure 2. (a) Chronopotential curve of Mg insertion into Mo_6S_8 and (b) the ex situ XRD patterns of the electrodes with a $Mg_xMo_6S_8$ ($x = 0$, 0.5, 1, 1.5, and 2) composition. The numbers of the XRD patterns correspond to the points on the chronopotential curve.

and the changes that occur in the crystal structure of the host with ion insertion.

Figure 2a shows such a chronopotential curve for the Mg−Mo_6S_8 system. The experiment was performed at 60 °C in order to avoid the problems of Mg diffusion in this host, such as the relatively slow kinetics of initial Mg insertion and Mg trapping upon the charge of the cell.[15,29−31] The lower and upper curves present the discharge and charge of the electrochemical cell, respectively. Two potential plateaus on the curves testify that the whole intercalation process includes two separate stages, and each of them involves two electrons. Thus, Mg insertion into Mo_6S_8 results in the formation of new phases with $MgMo_6S_8$ and $Mg_2Mo_6S_8$ stoichiometry. The process can be described by eqs 1 and 2, and each reaction occurs at its characteristic electrochemical potential, equal to ∼1.4 and 1.1 V, respectively. As will be shown below, these potentials are related to the occupation of the inner and outer sites in the Mo_6S_8 crystal structure.

Figure 2b presents the ex situ XRD patterns of the electrodes obtained at different intercalation levels. The pattern numbers correspond to the points of the chronopotential curve in Figure 2a. Note that a full theoretical capacity (four electrons) is realized in the electrochemical process. As a result, the total Mg amount in the electrodes (x in Mg_x-Mo_6S_8) can be determined very carefully by their electrochemical charge. According to the XRD patterns, the electrodes are composed of single phases for $x = 0$, 1, and 2 and a mixture of two phases for $x = 0.5$ and 1.5. Thus, the phase analysis confirms the mechanism of the electrochemical reactions presented in eqs 1 and 2 and is fully consistent with the experimental results of this work presented below.

Energy of States. *Calculational Methods.* Ab initio calculations were done using density functional theory plane-wave-based methods, within the generalized gradient approximation (GGA) as parametrized by Perdew et al.[36,37] The core and valence electrons were treated by the projector-augmented-wave method.[38−40] The calculations have been performed using ab initio total energy and the molecular dynamics program VASP (Vienna ab initio simulation program) developed at the Institut für Materialphysik of the Universität Wien.[41−44] Calculations are done with a plane-wave cutoff of 364 eV and a $2 \times 2 \times 2$ Monkhorst-Pack k-point mesh, and the ions are relaxed until the total energy converged to within better than 1 meV per atom. No temperature or zero point effects are included in the ab initio calculations.

Electrostatics. As a qualitative assessment of the likely stable sites, we examined the electrostatic energies of different possible cation arrangements. We used unscreened Coulomb interactions evaluated with the Ewald summation technique.[45] We considered charges of +1 and +2 on the intercalated cations, fixed the S anion to be −2, and allowed the Mo valence to adjust to give a charge-neutral cell. The atom positions were fixed and taken from those refined for $Li_4Mo_6S_8$.[20]

Electrostatic energies were calculated for all possible arrangements of 1 and 2 cations on the sublattices of Li sites within a single primitive cell of the $Li_4Mo_6S_8$ structure. For a single cation with charge +1 or +2, the inner ring sites were found to be more stable than the outer ring sites. This is consistent with the occupations seen in both $Li_1Mo_6S_8$[20] and $Cu_{1.8}Mo_6S_8$,[25] in which the cations occupy the inner ring. The results are also consistent with the stability of Mg in the inner ring in $Mg_1Mo_6S_8$ found experimentally in this work. This suggests that simple electrostatic interactions with the host help drive the stability of the inner ring over the outer ring, perhaps because of the short separation between Mo and the outer ring.

Electrostatic calculations for two cations show different results for +1 and +2 cations. The most stable arrangement for +1 cations are on opposite sides of the inner ring, consistent with the low-temperature arrangement seen experimentally for Cu cations.[46] However, this is different from the Li results of Ritter et al., which suggest that for two Li+ cations, both the inner and outer rings are occupied.[20] For two +2 cations, the most stable electrostatic arrangement was found to be one cation on the inner sites and one as far away as possible on the outer sites. Thus, it is clear that the electrostatic repulsion between the cations is enough to overwhelm the greater stability of the inner site and drive one of the cations to the outer site. This result is fully consistent with what is seen experimentally in this work for $Mg_2Mo_6S_8$.

(36) Perdew, J. P.; Burke, K.; Ernzerhof, M. *Phys. Rev. Lett.* **1996**, *77*, 3865.
(37) Perdew, J. P.; Burke, K.; Ernzerhof, M. *Phys. Rev. Lett.* **1997**, *78*, 1396.
(38) Blochl, P. E. *Phys. Rev. B* **1994**, *50*, 17953.
(39) Kresse, G.; Hafner, J. *J. Phys. C: Condens. Matter* **1994**, *6*, 8245.
(40) Kresse, G.; Joubert, D. *Phys. Rev. B* **1999**, *59*, 1758.
(41) Kresse, G.; Hafner, J. *Phys. Rev. B* **1993**, *47*, 558.
(42) Kresse, G.; Hafner, J. *Phys. Rev. B* **1994**, *49*, 14251.
(43) Kresse, G.; Furthmüller, J. *Comput. Mat. Sci.* **1996**, *6*, 15.
(44) Kresse, G.; Furthmuller, J. *Phys. Rev. B* **1996**, *54*, 11169.
(45) Allen, M. P.; Tildesly, D. J. *Computer Simulation of Liquids*, Oxford Science Publishers: New York, 1989.
(46) Chevrel, R.; Sergent, M.; Prigent, J. *Mater. Res. Bull.* **1974**, *9*, 1487.

Table 1. Energies for Different Arrangements of the Mg Atoms in $Mg_1Mo_6S_8$.

initial position for one Mg atom	energy (meV/FU)	site coordinates (hexagonal setting)	ref
Mg1 site	0	(0.699, 0.440, 0.327)	this work
inner site	2	(0.686, 0.450, 0.322)	20
center cavity 2	246	(0, 0.5, 0.5)	21, 23
outer site	275	(0.178, 0.290, 0.865)	20
center cavity 1	284	(0, 0, 0)	1, 2

Table 2. Energies for Different Arrangements of the Mg Atoms in $Mg_2Mo_6S_8$.

initial position for two Mg atoms	site occupation, Mg1−Mg2	energy (meV/FU)	site coordinates (hexagonal setting)
outer sites	outer−outer	0	(0.686, 0.450, 0.322) (0.845, 0.623, 0.198)
Mg1−Mg2 sites	inner−outer	31	(0.732, 0.462, 0.332) (0.162, 0.306, 0.874)
perturbed ES +2	inner−outer	32	(0.686, 0.450, 0.322) (0.290, 0.112, 0.135)
ES +2	inner−outer	39	(0.686, 0.450, 0.322) (0.779, 0.155, 0.198)
ES +1	inner−inner	100	(0.686, 0.450, 0.322) (0.981, 0.883, 0.011)
Cu sites	inner−inner	389	(0.822, 0.428, 0.337) (0.178, 0.572, 0.663)

Table 3. Comparison between the Experimental Atomic Coordinates in the Crystal Structures of $Cu_{1.80}Mo_6S_8$ and $MgMo_6S_8$.

compd	atom Wyckoff	*X*	*Y*	*Z*	occupancy	ref
$Cu_{1.80}Mo_6S_8$	Mo	0.0159	0.1690	0.3890	1	25
$MgMo_6S_8$	18f	0.0163(2)	0.1714(1)	0.3932(1)	1	this work
$Cu_{1.80}Mo_6S_8$	S_1	0.3097	0.2769	0.4118	1	25
$MgMo_6S_8$	18f	0.3173(4)	0.2809(4)	0.4118(3)	1	this work
$Cu_{1.80}Mo_6S_8$	S_2	0	0	0.2015	1	25
$MgMo_6S_8$	6c	0	0	0.2115(6)	1	this work
$Cu_{1.80}Mo_6S_8$	Cu 18f	0.7266	0.4839	0.3291	0.26	25
$MgMo_6S_8$	Mg 18f	0.699(6)	0.440(3)	0.327(3)	0.167	this work

The electrostatic results are qualitative, but suggest some useful rules for thinking about site occupancies in the Chevrel structure. Electrostatically, the site occupancy can be thought of as a balance between two tendencies, the electrostatic field, which stabilizes cations in the inner sites, and the intercalated cation−cation repulsive interactions, which drive the cations apart, keeping all of them from residing in the inner sites. The strength of the cation−cation interactions obviously increases from +1 to +2 cations and changes the electrostatic ground state for two cations from being within the inner sites, to occupying one inner and one outer site. The agreement with experimental trends suggests that electrostatics plays an important role. However, to include more realistic physics, we now show results from full ab initio calculations.

Ab initio Calculations. When we relaxed cations in the Chevrel structure, we found many local minima, giving different energies for even very similar initial structures. Therefore, we will carefully specify our method for determining starting positions. First, the Mo_6S_8 lattice was fully relaxed, and these relaxed coordinates were used as the initial host positions for all calculations. The specific initial Mg positions were determined as described below.

For a single Mg atom, we considered five possible arrangements within the primitive rhombohedral cell (Table 1). These corresponded to an inner site, outer site, the experimental Mg position found for $Mg_1Mo_6S_8$ in this work (Mg1 site in Table 1), the center of cavity 1, and the center of cavity 2. The latter two positions are fixed by symmetry and may be found for relatively big cations such as Ag^+ and Pb^{2+} (cavity 1)[1,2] or Mn and Cr (cavity 2),[21] whereas the first two were determined by using the fractional coordinates of Li from $Li_4Mo_6S_8$.[20] The experimental Mg position is given in this paper in Table 3. The final energies after full relaxation are given in Table 2, with the most stable arrangement set to zero.

It is clear that the ab initio results predict a significantly more stable inner site than outer site. This is consistent with the electrostatic results and the experimental findings in this work. In addition, the shifting of the center of cavity 1 to allow for additional relaxations is clearly important for the Mg case, consistent with what has been seen previously for the Li and Cu atoms, as well as for the experimental results of this work.

For two Mg atoms per formula unit, there are many more possible starting positions that one might explore. We considered six different initial configurations for the Mg positions, guided by previous experiments and our calculated results described above. Unless explicitly stated, the positions were taken from the fractional coordinates of Li from $Li_4Mo_6S_8$.[20] Two starting positions correspond to the electrostatic ground states for +1 (ES +1) and +2 (ES +2) cations found above. A third initial configuration simply perturbed the ES +2 structure to move the outer site Mg to the farthest outer site possible within the other half of the outer site dumbbells (the outer sites come in pairs of "dumbbells", and we simply switched the outer Mg to the orbit of the other member of the dumbbell pair and then took the site farthest from the inner Mg) (perturbed ES+2).

The next initial configuration took the Mg atoms to be at the fractional positions of the two Cu atoms in low-temperature $Cu_{1.8}Mo_6S_8$ (Cu sites in Table 2).[25] Also, we arranged the Mg in two outer sites, kept as far apart as possible (within a single primitive cell), leaving the inner sites empty (outer sites in Table 2). Finally, we used the experimental Mg position found for $Mg_2Mo_6S_8$ in this work (Mg1−Mg2 sites in Table 2). These initial arrangements include the most likely structures suggested by electrostatic energies, single Mg ab initio energies, and experiments. Note that we do not even consider the cavity centers, because they seemed to be quite unstable. The starting fractional coordinates and, after full relaxation, the final energies, are given

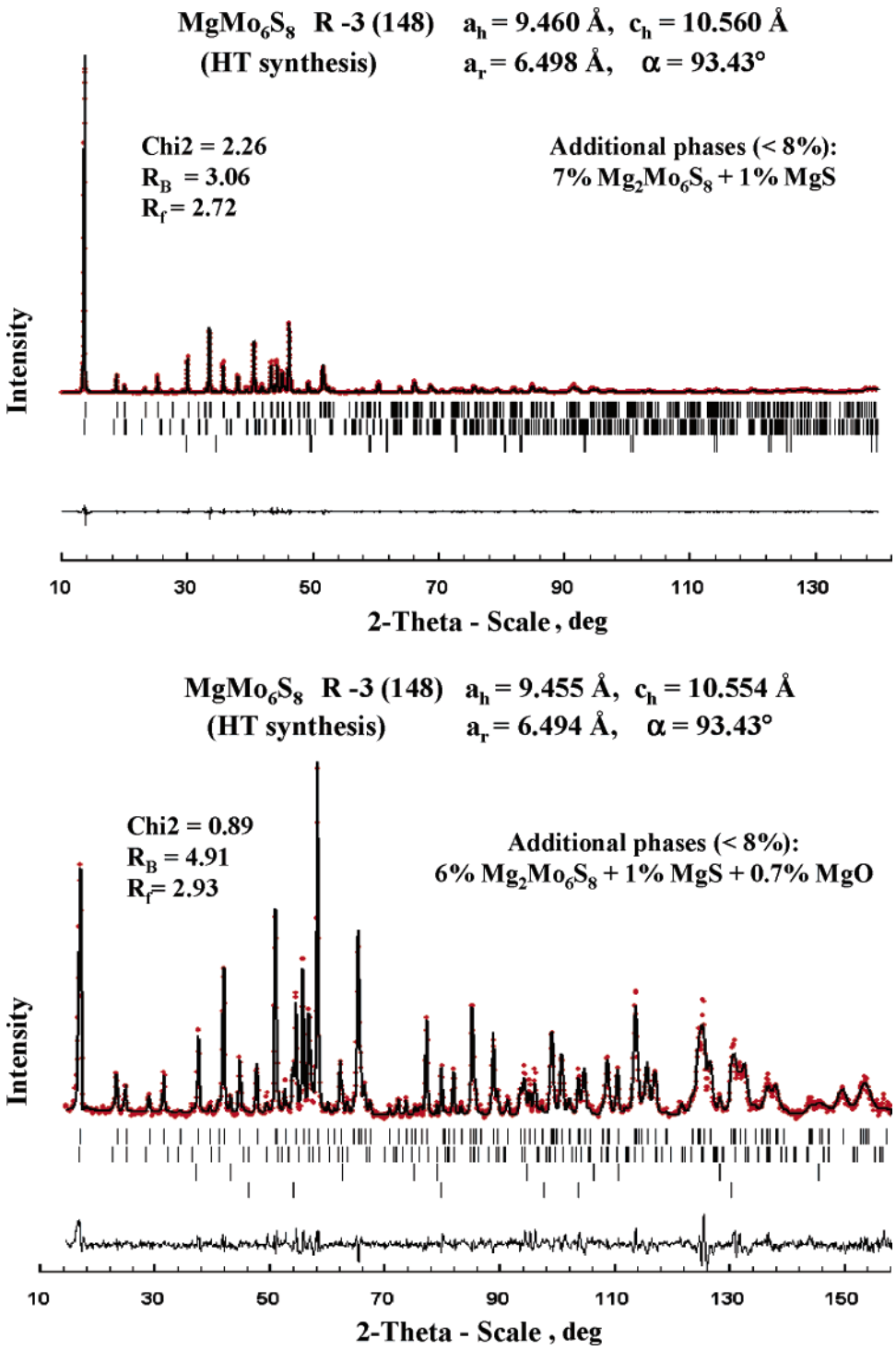

Figure 3. Rietveld refinement for $MgMo_6S_8$: (a) XRD profiles and (b) neutron diffraction profiles.

in Table 2, with the most stable arrangement set to zero. In each case, we also note how many inner and outer sites are occupied.

These results predict that the most stable arrangement for Mg is to occupy two outer sites. However, the calculations are for zero temperature, and the thermal effects may drive more Mg into the inner sites, as this will increase the configurational entropy. The partial occupation of inner sites is additionally supported by the relatively close energy of the different inner−outer site arrangements, which suggests that excitations of inner site occupancy can occur with relatively little energy cost. The two inner−inner arrangements are significantly higher in energy, presumably due to the electrostatic interactions between the Mg. Surprisingly, although both ES +1 and the Cu site arrangements involve two inner sites being occupied, they give quite different energies. This is an example of how similar site occupancies can find different local minima.

There is one previous ab initio study on $Mg_xMo_6S_8$ of which we are aware.[27] We agree with these results in our prediction that the center site of cavity 1 is not stable for Mg. However, our results do not agree with their prediction of nearly degenerate occupancy of the inner and outer rings for $Mg_1Mo_6S_8$ and preferential occupancy of the inner ring

Table 4. Comparison between Interatomic Distances (Å) in the Crystal Structures of $Mg_xMo_6S_8$ ($x = 1$ and 2) and $Cu_xMo_6S_8$ ($x = 1.8$ and 3.6)[a]

distance	$MgMo_6S_8$	$Mg_2Mo_6S_8$		$Cu_{1.8}Mo_6S_8$	$Cu_{3.6}Mo_6S_8$
Mo−Mo	2 × 2.683(2)	2 × 2. 658(7)	2.669(5)*	2.683	2.659
	2 × 2.735(2)	2 × 2.667(8)	2.689(6)*	2.752	2.681
	3.218(2)	3.411(6)	3.365(5)*	3.237	3.389
Mo−S1	2.431(4)	2.408(11)	2.434(9)*	2.407	2.443
	2.445(4)	2.423(10)	2.435(9)*	2.443	2.479
	2.499(4)	2.533(12)	2.476(10)*	2.478	2.502
	2.503(4)	2.633(10)	2.580(8)*	2.494	2.551
Mo−S2	2.465(5)	2.495(13)	2.486(9)*	2.469	2.491
Mo−Mg1(Cu1)	3.46(6)	3.44(5)	3.41(3)*	3.163	3.250
Mo−Mg2(Cu2)		2.84(4)	2.97(2)*	−	3.074
Mg1(Cu1)−S1	2.43(5)	2.26(3)	2.42(2)*	2.321	2.390
	2.57(3)	2.71(5)	2.55(3)*	2.343	2.399
	3.26(5)	3.24(5)	3.45(3)*	3.473	3.590
Mg1(Cu1)−S2	2.34(3)	2.32 (3)	2.42(2)*	2.382	2.421
	2.47(3)	2.51 (3)	2.44(2)*	2.456	2.437
Mg1−Mg1 (Cu1−Cu1)	2 × 0.91(8)	2 × 1.14(7)	1.12(4)*	2 × 1.261	2 × 1.276
	2 × 1.55(7)	2 × 1.95(5)	1.94(3)*	2 × 2.180	2 × 2.210
	1.80(4)	2.26(4)	2.24(3)*	2.518	2.552
Mg1−Mg2 (Cu1−Cu2)		2.25(5)	2.02(3)*		1.426
		2.65(6)	2.46(3)*		1.823
		2.72(6)	2.72(3)*		2.424
		2.78(5)	2.87(3)*		2.887
		3.08(6)	3.39(3)*		3.285
		3.37(6)	3.40(3)*		3.299
Mg2 (Cu2)−S1		2.25(4)	2.33(2)*		2.415
		2.38(4)	2.38(2)*		2.319
		2.66(4)	2.52(2)*		2.529
		2.88(4)	3.01(2)*		3.349
		3.73(4)	3.71(2)*		3.484
Mg2(Cu2)−S2		2.57(3)	2.55(2)*		2.274
		3.14(3)	3.19(2)*		3.625
Mg2−Mg2 (Cu2−Cu2)		0.69(5)	0.93(3)*		2.067
		2 × 3.84(7)	2 × 3.85(3)*		2 × 3.025
		2 × 4.29(7)	2 × 4.26(3)*		2 × 3.570
S1−S1	2 × 3.399(6)	2 × 3.43 (1)	2 × 3.45 (1)*	2 × 3.353	2 × 3.424
	2 × 3.502(6)	2 × 3.58(1)	2 × 3.57(1)*	2 × 3.513	2 × 3.514
	2 × 3.600(5)	2 × 3.58(1)	2 × 3.59(1)*	2 × 3.569	2 × 3.625
	3.829(6)	3.81(1)	3.78(1)*	3.775	3.748
S1−S2	3 × 3.390(5)	3 × 3.50(1)	3 × 3.49(1)*	3 × 3.353	3 × 3.424
	3 × 3.543(5)	3 × 3.53(1)	3 × 3.56(1)*	3 × 3.513	3 × 3.514
	3 × 3.603(4)	3 × 3.80(1)	3 × 3.77(1)*	3 × 3.569	3 × 3.625

[a] The values marked by stars were obtained using soft distance constraints upon fitting.

for $Mg_2Mo_6S_8$. Differences in pseudopotentials, exchange-correlation functions, and other numerical issues may account for some of this discrepancy. However, we think it also possible that the earlier calculations did not find the optimally relaxed positions for some configurations, since this system easily gets caught in suboptimal local minima during relaxation. As our calculations agree better with the experimental results reported in this work, we believe that we present a more accurate prediction.

Rietveld Refinement of the MgCP Crystal Structures Based on X-ray and Neutron Diffraction. *$MgMo_6S_8$.* As is clear from the previous sections, there are two opposite models of the $MgMo_6S_8$ crystal structure, which differ by the positions of the Mg^{2+} ions: only inner sites according to our calculations (model 1), and both of the sites (inner and outer) in the work of Kganyago et al. (model 2). Hence, in order to determine the Mg^{2+} ion location, both of the models were used as the initial ones in the refinement procedure. However, it should be mentioned that Model 2 was not completely identical to the crystal structure proposed by Kganyago et al. because the triclinic symmetry stated by the authors has not been confirmed in previous experiments.[15] Thus, both of the models were based on the rhombohedral symmetry $R\bar{3}$, the unit-cell parameters obtained in the previous work,[15] and the atomic positions known for the CPs with small cations.[1]

Panels a and b of Figure 3 present the X-ray and neutron Rietveld profiles, respectively. Here, model 1 was used in the refinement. According to the quantitative analysis, the amount of $MgMo_6S_8$ in the sample under study was greater than 92%. The impurities (6% $Mg_2Mo_6S_8$, 1% MgS, and 0.7% MgO) found in this sample were related to the high Mg concentration in the initial mixture (see the Experimental Section). The atomic thermal parameters (0.33 Å^2 for Mo, 0.5 Å^2 for S, and 1 Å^2 for Mg) were chosen according to the literature data[46,2] and remained constant. The refinement of the peak shape and asymmetric parameters showed that their values for all the phases were similar or close to that of the standards (highly crystalline cubic materials) measured under the same experimental conditions. Thus, the material under study is also highly crystalline.

Initially, the X-ray and neutron profiles were refined separately, but because of the very close results, at a last stage of the refinement, they were combined (multipattern refinement). Such a combination allows for the attainment of atomic positions suitable for both X-ray and neutron diffraction experiments for the same material. The R-factors of both the patterns in the multipattern refinement were very

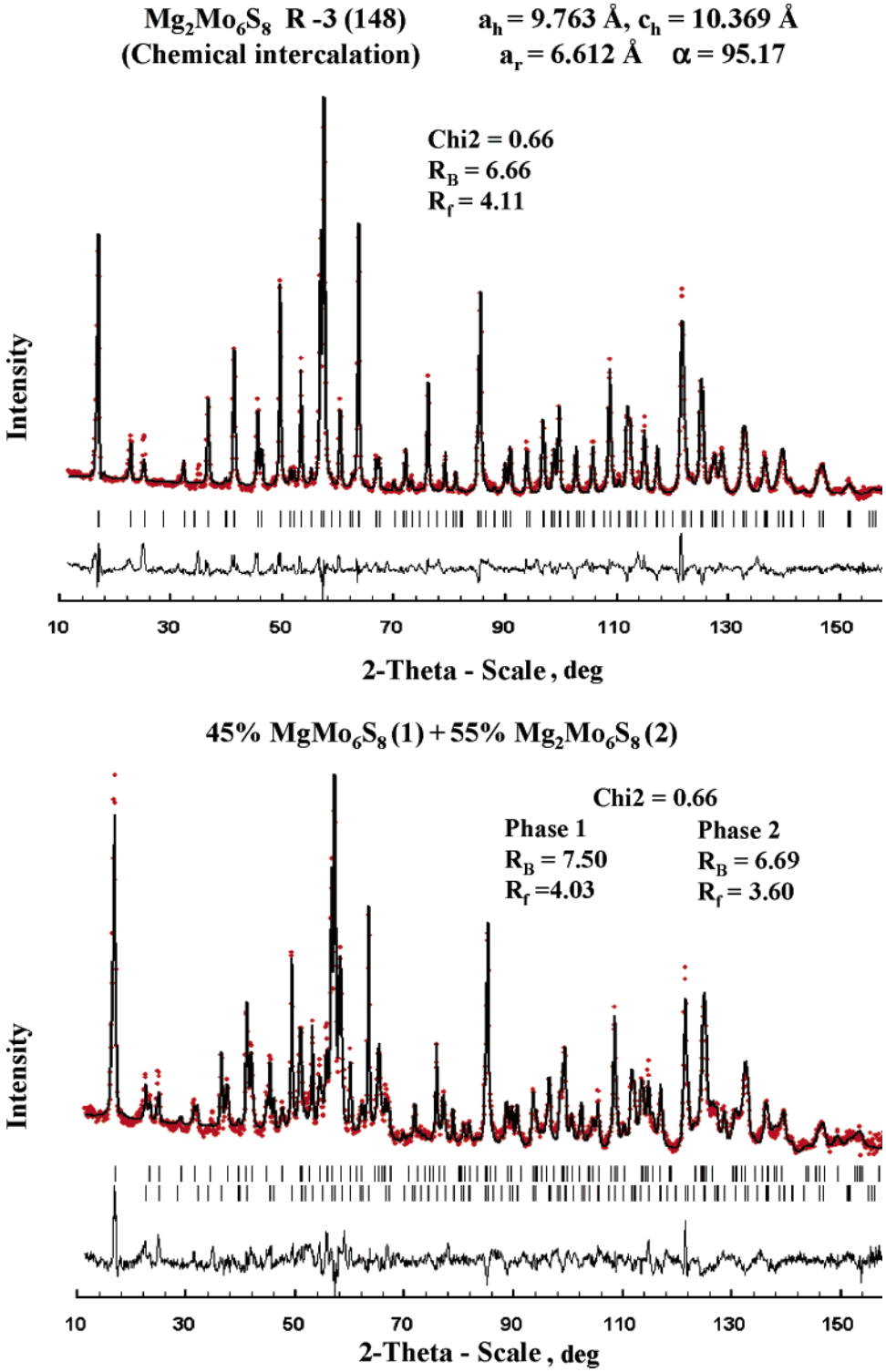

Figure 4. Rietveld refinement of the neutron diffraction profiles: (a) $Mg_2Mo_6S_8$ and (b) a mixture of $Mg_2Mo_6S_8$ and $MgMo_6S_8$.

close to the initial ones, whereas the global factor (Chi2 = 1.58) was equal to their average value.

Table 3 compares the atomic positions (with standard deviations indicated in parentheses) in the crystal structure of $MgMo_6S_8$ and $Cu_{1.80}Mo_6S_8$.[25] The latter material was chosen for the comparison because of close XRD patterns and a similar electrostatic charge of the cluster, but such a choice is not crucial: As is known from the literature,[1,2] the Mo and S locations, as well as the position of the inner and outer sites, are relatively constant for CPs with different small cations because of the rigid structure of the Mo_6S_8 cluster and similar electrostatic interactions between the cluster framework and different cations.

The atomic positions, obtained by the combined refinement, were used to calculate the interatomic distances and their standard deviations for $MgMo_6S_8$ (Table 4). As can be seen from their comparison with the same distances in other CPs, the values, obtained by the refinement, are reasonable enough to be used in the analysis of the Mg^{2+} ion's motion upon intercalation (see below). The bond valence sum,

Table 5. Results of Multipattern Refinement of the Mg Positions in $Mg_2Mo_6S_8$ for Different Models

		initial parameters		refined parameters		R-factors		
model	Mg site	Mg position	occupancy	Mg position	occupancy	Chi2	RB(1) Rf(1)	RB(2) Rf(2)
		0.724		0.723(3)				
	inner	0.483	0.167	0.465(2)	0.168(6)			
I		0.332		0.335(2)			6.66	6.69
		0.152		0.160(2)		0.67	4.11	3.6
	outer	0.241	0.167	0.290(2)	0.166(6)			
		0.892		0.857(2)				
		0.152		0.156(2)			12.11	8.3
II	outer	0.241	0.333	0.281(2)		1.02	7.14	4.78
		0.892		0.858(1)				
		0.724		0.724(2)			12.57	9.78
III	inner	0.483	0.333	0.480(2)		1.20	6.076	4.8
		0.332		0.334(1)				

calculated for the Mg^{2+} ion according to these distances (R_1 = 2.18 for the Mg−S pair),[47] is equal to 1.96, thus confirming the crystal structure solution.

In the case where the Mg^{2+} ions were located in both the inner and outer sites (model 2), all the R-factors were almost twice as high as that for the inner-site model. The refinement of the Mg^{2+} ion coordinates resulted in their shift to the inner sites. The refinement of the occupation number for the Mg^{2+} ions showed a negative value for the outer sites. Thus, according to the Rietveld analysis of the X-ray and neutron diffraction profiles, Mg^{2+} ions in $MgMo_6S_8$ are located in the inner sites.

$Mg_2Mo_6S_8$. The atmospheric instability of $Mg_2Mo_6S_8$ is higher than that of $MgMo_6S_8$. Moreover, the former material has the maximal Mg concentration; therefore, it cannot be obtained as the major phase in the passivated product, as was done for $MgMo_6S_8$. In fact, a maximal quantitative ratio of these two phases, $Mg_2Mo_6S_8$:$MgMo_6S_8$, obtained after the air stabilization, was about 2:1. Thus, the samples with the $Mg_2Mo_6S_8$ composition should be prepared and studied under special conditions without any oxidizing agent. We were able to ensure such conditions for relatively long-time measurements only for the product of chemical intercalation and only in the case of the neutron diffraction experiment, performed in a hermetically sealed vanadium container.

For $Mg_2Mo_6S_8$, three different models, which differ by the positions of the Mg^{2+} ions, may be proposed:

1) One ion occupies the inner site and another one, the outer site (Model 1). Such an arrangement is based on the cation distribution in classic CPs with small cations.

2) Both of the ions are related to the same outer ring (Model 2). Such an arrangement is probable according to our ab initio calculations.

3) Both of the ions are in the same inner ring (model 3). This model was proposed by Kganyago et al.[27]

All these models were verified by the refinement procedure. As in the previous case, the common characteristic features of the models were the rhombohedral symmetry, $R\bar{3}$, the unit-cell parameters obtained in the previous work,[15] and the atomic positions known for the CPs with small cations.[1]

In order to obtain more precise results, we completed the combined neutron refinement for two samples with different compositions: about 100 and 55% of $Mg_2Mo_6S_8$ (panels a and b, respectively, of Figure 4). The latter composition resulted from an unsuccessful attempt to prepare the unoxidized material. Panels a and b of Figure 4 correspond to model 1. In the case of models 2 and 3, the R-factors were essentially higher (Table 5). Moreover, the distribution of the Mg atoms, obtained by the refinement of their occupation number, corresponds to model 1: one Mg^{2+} ion per formula unit in the inner site and one Mg^{2+} ion in the outer site.

We have to mention that in the case of $Mg_2Mo_6S_8$, the R-factors were relatively high, even for model 1, because some weak diffraction peaks were not identified. They may be related to the phase under study or to some impurity. In any case, it is clear that these peaks cannot be caused by the triclinic distortion of $Mg_2Mo_6S_8$, but some kind of superstructure cannot be excluded.

In order to confirm the crystal structure solution, we verified the results of the neutron diffraction by X-ray diffraction. Figure 5 shows the Rietveld profile obtained for the air-stabilized material with the general composition, $Mg_2Mo_6S_8$. As was mentioned above, before stabilization, the Mg extraction from the crystal structure takes place. As a result, the material is mainly a mixture of $Mg_2Mo_6S_8$ (65%) and $MgMo_6S_8$ (35%). It is not clear where the Mg goes upon its extraction from the CPs during the material oxidation, but the amount of this Mg does not exceed 2 wt % (Table 6). Moreover, the Mg-containing phases formed upon oxidation might be amorphous or might dissolve upon the material treatment in THF.

As can be seen, the R-factors of the X-ray profile refinement were relatively low. However, the location of the Mg^{2+} ions in the $Mg_2Mo_6S_8$ crystal structure could not be established using only the XRD data, because there was no difference in the R-factors obtained for the different models. Nevertheless, the XRD analysis confirms that there is no triclinic distortion in the CP crystal structure upon Mg insertion.

Table 7 compares the atomic positions in the crystal structure of $Mg_2Mo_6S_8$ (the result of neutron diffraction) and $Cu_{3.66}Mo_6S_8$.[25] The former positions were used to calculate the interatomic distances (and their standard deviations, indicated in parentheses) for $Mg_2Mo_6S_8$ (Table 4). As can be seen, the values, obtained by the refinement, are consistent, but they may be improved by using soft distance constraints in the refinement procedure (values marked by stars in Tables 4 and 7). The bond valence sums, calculated for the Mg^{2+} ions according to these distances, are equal to

(47) Brese, N. E.; O'Keefee, M. *Acta Crystallogr., Sect. B* **1991**, *B47*, 192.

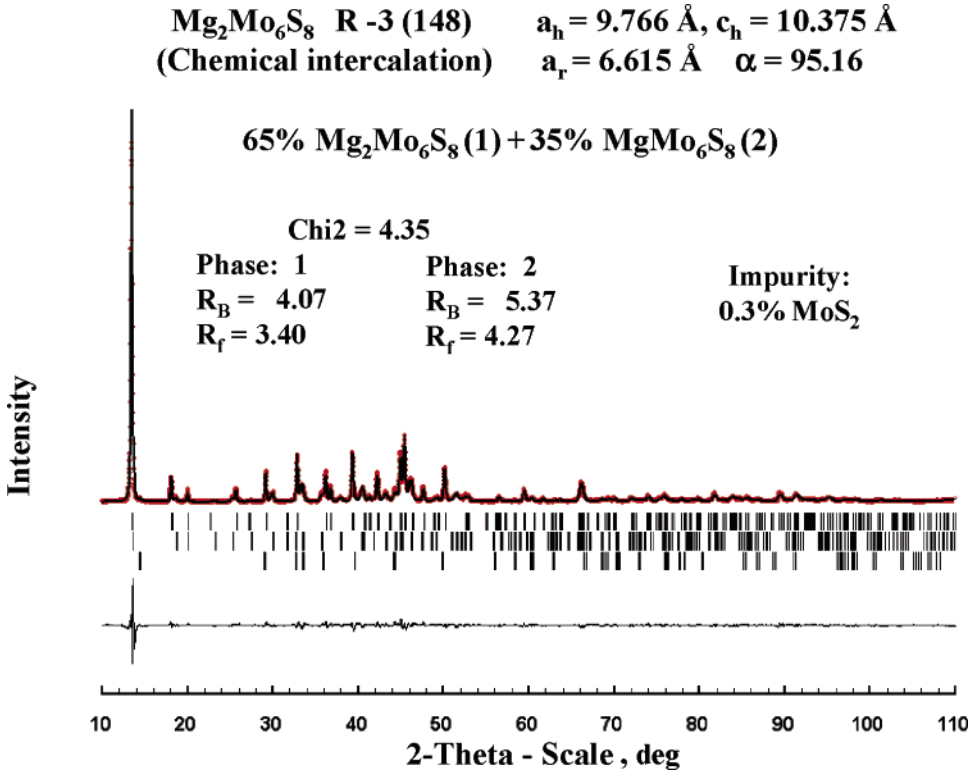

Figure 5. X-ray Rietveld profiles for $Mg_2Mo_6S_8$.

Table 6. Examples of the Mg Balance in the Materials Under Study

	$Mg_{1.5}Mo_6S_8$ (HT-product)		$Mg_2Mo_6S_8$ (chemical intercalation)	
composition	phase content (wt %)	Mg content (wt %)	phase content (wt %)	Mg content (wt %)
$Mg_2Mo_6S_8$	6	0.3	55	3.0
$MgMo_6S_8$	92.3	2.6	45	1.3
MgS	1	0.4	–	–
MgO	0.7	0.4	–	–
Σ expected	100	4.2	100	5.5
Σ experimental		3.7		4.3
Mg lack		0.5		1.2

1.91 and 2.02 for the Mg1 and Mg2 positions, respectively, thus confirming the crystal structure solution.

An analysis of the interatomic distances of Table 4 allows for an estimation of the reliability of each model, as discussed in this paper. In fact, according to the table, the distances, Mg1(inner site)−Mo and Mg2(outer site)−Mo are equal to ∼3.4 and ∼3.0 Å, respectively. Thus, the outer sites in the MgCPs are effectively closer to the Mo atoms. In the known CPs with similar cation distribution, the cation−Mo distance varies from 2.96 to 4.2 Å,[1,2] whereas the minimal value is related to NiCPs with possible metal−metal bonding between Ni and Mo atoms. It is clear that such bonding is improbable in the Mg case. The distance of 3.0 Å is equal to the sum of the metallic radii of Mg and Mo (1.6 and 1.4 Å, respectively). It can be regarded as a minimal Mg−Mo distance in crystal structures and should be associated with relatively strong repulsion between these cations. On the basis of these considerations, we can conclude that the inner sites are really more favorable for $MgMo_6S_8$ stoichiometry. Only the insertion of the second cation per formula unit and the subsequent repulsion between the Mg^{2+} ions result in the additional occupation of the outer site in $Mg_2Mo_6S_8$. Thus, in view of the energy of the cation sites, the crystal structure of Mg_x-Mo_6S_8 ($x = 1$ and 2) is similar to that of classic CPs, such as CuCPs.[1,2]

However, the comparison made in Table 7 demonstrates not only the similarity of the Mg and Cu containing sulfides but also their differences. As can be seen from Table 4, the inner ring in MgCPs is essentially smaller than that in CuCPs (compare the Mg1−Mg1 and Cu1−Cu1 distances). For instance, for MgCPs, the maximal distance between the inner sites in the ring is equal to 1.8 Å, which is close to the distance between Li^+ ions in $LiMo_6S_8$ (1.9 Å),[20] whereas the same distance in CuCPs is equal to 2.6 Å.[25] As was shown in the classic reviews,[1,2] the radius of the inner ring is a very important parameter for the CPs, which characterizes the delocalization of the cations from the center of cavity 1.

According to K. Yvon,[1] this parameter represents a mean radius of a circular cation movement around the origin of cavity 1. For instance, it was suggested that the energy of the thermal vibrations of the Cu^+ ions in the CP crystal structure is enough for their circuit motion even at room temperature.[1] The aim of the previous works devoted to the CPs was mainly to find the correlation between the cation delocalization and other structural parameters (like the Mo−Mo distances) or physical properties (like superconductivity).[1] However, it is clear that the delocalization relates directly to the distance between the cations sites, and that this parameter should be crucial for the cation mobility in the CPs.

As was shown,[1] the delocalization value depends mainly on the cation size: The larger the cation, the closer is its position to the center of cavity 1. Commonly, the delocalization correlates well with the angle α of the rhombohedral

Table 7. Comparison between the Experimental Atomic Coordinates in the Crystal Structures of $Cu_{3.66}Mo_6S_8$ and $Mg_2Mo_6S_8$[a]

compd	atom Wyckoff	*X*	*Y*	*Z*	occupancy	ref
$Cu_{3.66}Mo_6S_8$	Mo 18f	0.0142	0.1637	0.3928	1	25
$Mg_2Mo_6S_8$	Mo 18f	0.0136(6)	0.1641(5)	0.3955(4)	1	this work
	Mo 18f	0.0162(5)*	0.1665(4)*	0.3953(4)*	1	this work
$Cu_{3.66}Mo_6S_8$	S1 18f	0.3068	0.2778	0.4087	1	25
$Mg_2Mo_6S_8$	S1 18f	0.3090(9)	0.2701(8)	0.4078(10)	1	this work
	S1 18f	0.3052(8)*	0.2713(7)*	0.4048(8)*	1	this work
$Cu_{3.66}Mo_6S_8$	S2 6c	0	0	0.2015	1	25
$Mg_2Mo_6S_8$	S2 6c	0	0	0.2061(15)	1	this work
	S2 6c	0	0	0.2081(10)*		
$Cu_{3.66}Mo_6S_8$	Cu1 18f	0.7238	0.4827	0.3324	0.23	25
$Mg_2Mo_6S_8$	Mg1 18f	0.745(5)	0.466(3)	0.343(3)	0.167	this work
	Mg1 18f	0.723(3)*	0.465(2)*	0.335(2)*	0.167	this work
$Cu_{3.66}Mo_6S_8$	Cu2 18f	0.1516	0.2409	0.8920	0.333	25
$Mg_2Mo_6S_8$	Mg2 18f	0.165(4)	0.298(3)	0.841(4)	0.167	this work
	Mg2 18f	0.160(2)*	0.290(2)*	0.857(2)*	0.167	this work

[a] The values marked by stars were obtained using soft distance constraints upon fitting.

unit cell: The higher delocalization, the greater is the α.[1] The latter depends also on the amount of inserted cations. For instance, for $Li_xMo_6S_8$, α = 92.0° (x = 1) and 94.4° (x = 3 or 4),[20] whereas for $Cu_xMo_6S_8$, α = 94.9° (x = 1) and 95.6° (x = ∼3 or ∼4).[1] As can be seen, our results for Mg_x-Mo_6S_8 (α = 93.4° for x = 1 and 95.2° for x = 2) are not exactly in line with these simple rules. In fact, the size of the Cu^+ ion is effectively larger than that of the Mg^{2+} one (1 and 0.7 Å, respectively, for octahedral coordination), i.e., according to the classic model, the Mg delocalization should be higher, but in practice, it is lower because of the higher Mg−Mo repulsion. This means that the cation delocalization from the center of cavity 1 is affected not only by the size of cations but also by their character.

The difference between the Cu- and Mg-containing CPs is not restricted to only the different delocalization values. As was mentioned in the Introduction, the inner ring in CuCPs is able to adopt two cations. In contrast, in the Mg case, the second cation occupies the outer ring because of the stronger repulsion between divalent Mg^{2+} ions, as compared to monovalent Cu^+ ions.

MgCPs Crystal Structure and Ionic Mobility. In order to understand the peculiarities of the Mg^{2+} ion mobility found for the $Mg_xMo_6S_8$ cathodes,[15] namely the relatively slow Mg insertion kinetics and trapping for $0 < x < 1$ and the fast kinetics for $1 < x < 2$, it is necessary to analyze once again the interatomic distances in the materials under study. As was mentioned above, one of the characteristic features of these phases is a relatively small Mg delocalization from the center of cavity 1. As a result, a minimal distance between the inner sites (Mg1−Mg1) in the MgCPs is twice as short as that between the inner and outer sites (Mg1−Mg2), 0.9 and 2.0 Å, respectively (Figure 6). In addition, the outer sites are less favorable because of the Mo repulsion. As a result, the probability of the Mg hopping between the inner sites in $MgMo_6S_8$ is essentially higher than that between the inner and outer sites. This leads to the circuit cation motion, instead of the progressive diffusion in the bulk of the material, and slows the insertion kinetics.

A fast kinetics is possible only with the insertion of the second cation per formula unit because of the repulsion between the inserted cations. Thus, the latter parameter is crucial for the cation mobility in CPs. The repulsion between two Mg^{2+} ions (per formula unit) exists also upon extraction of the first Mg^{2+} ion from $Mg_2Mo_6S_8$. As a result, there is no kinetic problem in this stage of the electrochemical process. However, upon Mg deintercalation, when all cathode material transforms into $MgMo_6S_8$, most of the Mg^{2+} ions in $MgMo_6S_8$ move in a circular manner between the inner sites and there are no additional Mg^{2+} ions, which can ensure the progressive diffusion. As a result, an essential amount of the Mg^{2+} ions is trapped into the Mo_6S_8 host at room temperature. In order to overcome the activation energy barriers existing between the inner and outer sites and to complete Mg extraction from the sulfide, it is necessary to increase the energy of the thermal vibrations in the material by its heating. In fact, the trapping effect disappears in the case of the battery operation at 60 °C.[15]

As can be seen, the crystal structure solutions presented in this paper agree well with the electrochemical behavior of the $Mg_xMo_6S_8$ insertion electrodes. In contrast, it seems that it is impossible to explain the problems of ionic mobility in these materials on the basis of the models proposed in the work of K. R. Kganyago et al. In fact, according to the latter,[27] for x = 1, the probabilities of occupation for the inner and the outer sites are equal, whereas the inner sites are occupied for x = 2. In such a case, we should expect a fast transport of the Mg^{2+} ions in the sulfide host for $0 < x < 1$ and possible trapping for $1 < x < 2$, but such expectation is in contradiction with the experimental results.

Interestingly, in contrast to the sulfide case, the Mg insertion into the selenide host, Mo_6Se_8, leads to triclinic distortion of the rhombohedral crystal structure, as well as

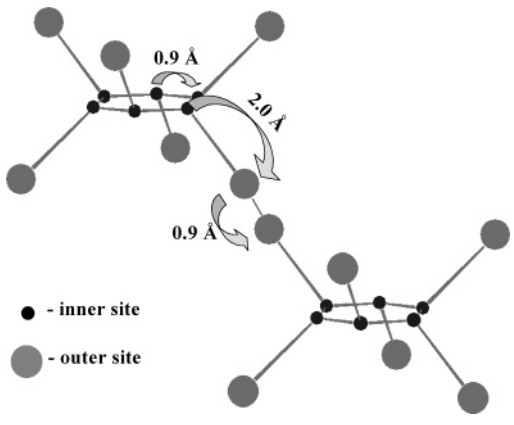

Figure 6. Arrangement of the cation sites in the $Mg_xMo_6S_8$ crystal structure.

to the changes in the cation site geometry.[48] As a result, the progressive Mg diffusion in the bulk becomes more favorable than the circuit motion, and the trapping effect is not realized. The relation between the crystal structure of the MgCPs with different composition and the Mg intercalation process is discussed in more detail in the second part of this work.[48]

Conclusion

The Mg insertion into Mo_6S_8 host happens in two stages

$$Mg^{2+} + 2e^- + Mo_6S_8 \rightarrow MgMo_6S_8$$

$$Mg^{2+} + 2e^- + MgMo_6S_8 \rightarrow Mg_2Mo_6S_8$$

A combination of the experimental (Rietveld analysis based on neutron and X-ray diffraction) and theoretical (calculation of the energy of states) methods was used to refine the MgCPs crystal structure, especially to determine the location of the Mg^{2+} ions. As was shown, the first stage of Mg insertion is associated with the occupation of the inner sites, whereas in $Mg_2Mo_6S_8$, one Mg^{2+} ion per formula unit is located in the inner sites and another one in the outer sites. Because of the statistic distribution of the cations between these sites, $Mg_xMo_6S_8$ ($x = 1, 2$) is crystallized in rhombohedral symmetry $R\bar{3}$: $a_r = 6.494$ Å, $\gamma = 93.43°$ for $x = 1$ and $a_r = 6.612$ Å, $\gamma = 95.17°$ for $x = 2$. The peculiarities of the MgCP crystal structures explain the Mg trapping that occurs in the material upon the electrochemical process.

Acknowledgment. Partial support for this work was obtained from the Israel−US Binational Foundation (BSF). The Institut Laue Langevin is warmly acknowledged for providing the neutron facilities. We wish to express our deep gratitude to Prof. A. Pron and Dr. D. Djurado for their assistance and interest during the performance of experiments.

Supporting Information Available: Crystallographic information in the form of a cif file. This material is available free of charge via the Internet at http://pubs.acs.org.

CM061656F

(48) Levi, E.; Lancry, E.; Mitelman, A.; Aurbach, D.; Isnard, O.; Djurado, D. *Chem. Mater.* **2006**, *18*, 3705.